

3 Theoretical framework

After choosing the Ronchi deflectometry experimental technique and generally describing some of its main abilities and limitations, the theoretical fundamentals of the Ronchi test technique are going to be discussed, from the adequate theoretical model to be used in its description to the data which needs to be extracted from the recorded intensity pattern in order to achieve the topographic reconstruction of a sample surface.

Since the early days of the Ronchi test, geometrical and physical explanations have been used to establish the nature of the registered fringes [Ronchi 1964]. Section 3.1 deals with the description of the physical model, which takes into account the effects of diffraction in the registered data and has been named diffractive theory of the Ronchi test. Section 3.2 will discuss the geometrical optics approach to the Ronchi test. However, under certain experimental conditions that will be specified next, both models will be shown to be equivalent. This will allow us to interpret the fringes as a

shadow pattern of the lines on the ruling. Section 3.3 will describe how to measure the surface under test from the data obtained using the Ronchi test.

3.1 Diffractive theory of the Ronchi test

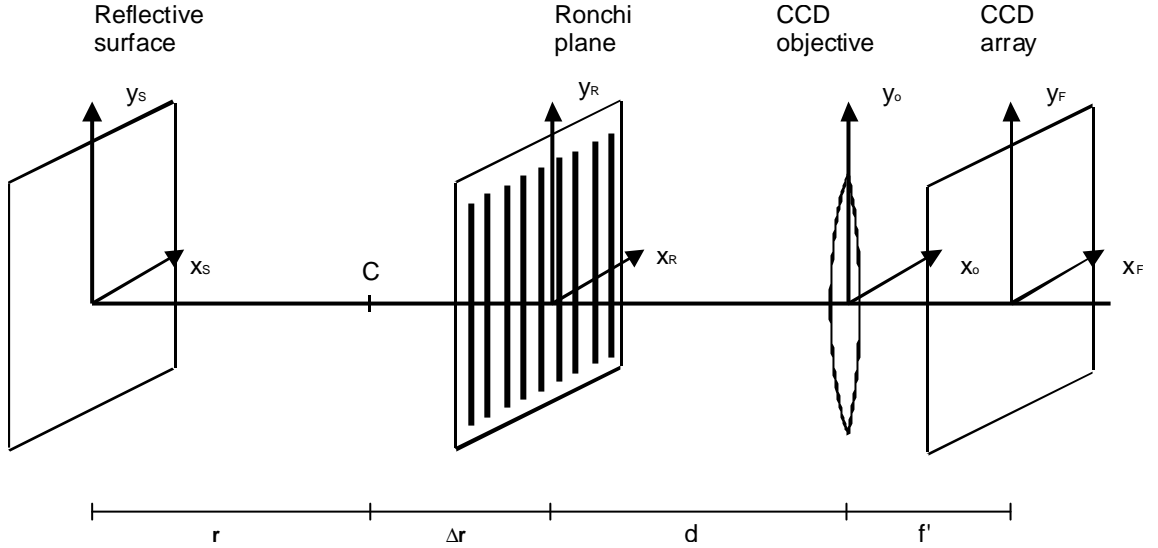
As a grating consisting of series of parallel lines, the Ronchi test may be considered as being a (low frequency) diffraction grating. This means we must take into account how important these diffractive effects will be in the recorded intensity pattern.

3.1.1.- The Ronchi test as a diffraction grating

We shall assume an experimental setup where a wavefront coming from a sample under test hits a Ronchi ruling, and the resulting intensity pattern is then recorded on the focal plane of a CCD camera with its objective pointing at infinity. We shall assume that under usual experimental conditions, the sample may be assumed to be very close to the plane tangent to the tested surface at its vertex. We shall define a set of coordinate systems as described in Fig.3.1.1, where the reference systems will be named $X_S Y_S$ at the plane tangent to the sample surface at its vertex; $X_R Y_R$ at the plane where the Ronchi ruling is placed (usually called the Ronchi plane); and $X_f Y_f$ at the focal plane of the lens. As the Ronchi ruling will not in general be placed at the center of curvature of the wavefront, the distance from the vertex of the surface to the Ronchi ruling is $r+Dr$, r being the radius of curvature of the ideal wavefront leaving the system under test, and Dr the amount of defocus. A finite distance d is assumed from the Ronchi plane to the entrance pupil of the CCD camera objective, described by its focal length. The ruling has light and dark slits of equal size, T being its period. That is, its transmittance has a square-wave profile.

The mathematical treatment we will describe will assume positive values for the defocus Dr , as this will be the usual configuration in our experimental setup. This means that the intensity pattern resulting from the propagation of the wavefront from the tangent plane to the surface to the Ronchi plane cannot be calculated through classical propagation integrals, as the wavefront will be passing through a singular point at $z=r$ (C point at Fig.3.1.1). The positive Dr means that our setup involves placing the Ronchi ruling "out of focus" from the wavefront.

Fig. 3.1.1: Reference systems used to develop the diffractive theory of the Ronchi test



The classic mathematical treatment of the Ronchi test usually assumes negative or null values for D_r (that is, "in focus" or "at focus" positions of the Ronchi test). This kind of treatment is used by some authors [Adachi 1963] [Cornejo 1992], giving very similar conclusions to those we will reach in our "out of focus" treatment.

As a starting point, we will use the complex amplitude incident on the Ronchi plane. We will use the propagation integral under the Fresnel approximation in order to obtain the complex amplitude distribution on the CCD array plane. We shall call the incident complex amplitude $U_R(x_R, y_R)$. The Ronchi ruling may be interpreted as a spatial filter placed on the $X_R Y_R$ plane. Let $T(x_R, y_R)$ be its transmittance. The complex amplitude leaving the Ronchi plane will therefore be

$$U'_R(x_R, y_R) = U_R(x_R, y_R) \cdot T(x_R, y_R) \quad (3.1.1)$$

It is a well known result of Fourier theory [Goodman 1968] that the complex amplitude distribution on the focal plane of a lens with an object placed a distance d in front of it can be written as

$$U_{\text{IMG}}(x_{\text{IMG}}, y_{\text{IMG}}) = \frac{e^{i \frac{k}{2f'} (1 - \frac{d}{f'}) (x_{\text{f}}^2 + y_{\text{f}}^2)}}{i \lambda f'} \text{FT} \left[U'_{\text{OBJ}} \left(\frac{x_{\text{OBJ}}}{\lambda f}, \frac{y_{\text{OBJ}}}{\lambda f} \right) \right] \quad (3.1.2)$$

where the FT symbol stands for Fourier transform, $X_{\text{IMG}} Y_{\text{IMG}}$ is the reference system on the focal plane of the lens, and $X_{\text{OBJ}} Y_{\text{OBJ}}$ is the reference system on the object plane.

According to the defined reference systems of Fig.3.1.1, $X_{\text{IMG}}Y_{\text{IMG}}$ is coincident with X_fY_f .

By applying this result to our development, and placing $U'_R(x_R, y_R)$ as the object plane complex amplitude,

$$U_f(x_f, y_f) = \frac{e^{\frac{i}{2f'}(1-\frac{d}{f'})(x_f^2+y_f^2)}}{i\lambda f'} \int_{-\infty}^{\infty} \int_{-\infty}^{\infty} dx_R dy_R U'_R(x_R, y_R) e^{-i\frac{2\pi}{\lambda}(x_R \frac{x_f}{f'} + y_R \frac{y_f}{f'})} \quad (3.1.3)$$

So through Eq. 3.1.1

$$U_f(x_f, y_f) = \frac{e^{\frac{i}{2f'}(1-\frac{d}{f'})(x_f^2+y_f^2)}}{i\lambda f'} \int_{-\infty}^{\infty} \int_{-\infty}^{\infty} dx_R dy_R \cdot U_R(x_R, y_R) \cdot T(x_R, y_R) \cdot e^{-i\frac{2\pi}{\lambda}(x_R \frac{x_f}{f'} + y_R \frac{y_f}{f'})} \quad (3.1.4)$$

It may be shown that the transmittance of the Ronchi Ruling (a square wave profile, with light and dark strips of equal size), can be expressed in terms of the Fourier series

$$T(x_R, y_R) = \sum_{n=-\infty}^{\infty} B_n e^{i\frac{2\pi n}{T}x_R} = \sum_{n=-\infty}^{\infty} (-1)^n \frac{\sin(\frac{n\pi}{2})}{n\pi} e^{i\frac{2\pi n}{T}x_R} \quad (3.1.5)$$

Lines have been assumed to run parallel to the Y axis, as shown in Fig. 3.1.1. Including 3.1.5 in 3.1.4 yields

$$U_f(x_f, y_f) = \frac{e^{\frac{i}{2f'}(1-\frac{d}{f'})(x_f^2+y_f^2)}}{i\lambda f'} \sum_{n=-\infty}^{\infty} B_n \int_{-\infty}^{\infty} \int_{-\infty}^{\infty} dx_R dy_R U_R(x_R, y_R) e^{-i\frac{2\pi}{\lambda f'} \left[x_R(x_f - \frac{n\lambda f'}{T}) + y_R \frac{y_f}{f'} \right]} \quad (3.1.6)$$

So we might write

$$U_f(x_f, y_f) = \frac{e^{\frac{i}{2f'}(1-\frac{d}{f'})(x_f^2+y_f^2)}}{i\lambda f'} \sum_{n=-\infty}^{\infty} B_n \cdot u_f\left(\frac{1}{\lambda f'}\left(x_f - \frac{n\lambda f'}{T}\right), \frac{y_f}{\lambda f'}\right) \quad (3.1.7)$$

where $u_f(x_f, y_f)$ stands for the Fourier transform of $U_R(x_R, y_R)$.

That is, the complex amplitude in the focal plane of the CCD camera is described as a phase term dependent on the coordinates of the observation point, that will be removed when making intensity measurements; a scaling factor on the total amplitude, dependent both on the wavelength and on the focal length of the objective being used; and a superposition of an infinity of sources with a distribution in the form of the Fourier transform of the complex amplitude incident on the Ronchi ruling, scaled

and sheared between them a distance $\frac{n\lambda f'}{T}$ along the X_f axis. Each of these sources has different amplitude B_n , which decreases with n .

When working in "at focus" or "in focus" setups, direct information from the wavefront present at the plane tangent to the surface may be taken into account in the equations. The main difference with the "out of focus" approach presented here (except some constant phase and scaling terms) is the consideration of the propagation from the tangent plane to the surface to the Ronchi plane. This entails an additional propagation integral, which leaves Eq.(3.1.7) as a superposition of the complex amplitude distribution at the plane tangent to the surface sheared along X_f the value $\frac{n\lambda f'}{T}$. This approach is common in the bibliography, but does not fit with the "out of focus" configuration usual in our experimental setup.

3.1.2.- The Ronchi test as a lateral shearing interferometer

From Eq.3.1.7, it follows that the Ronchi test may be interpreted as a lateral shearing interferometer, as many laterally sheared images of the incident wavefront appear in the observation plane giving rise to a number of fringes.

In order to reduce the number of diffracted orders, some authors use a sinusoidal fringe pattern, which gives $B_n=0$ coefficients except for B_{-1}, B_0 and B_1 [Schwider 1981]. It must be noticed that the amount of shear introduced using common Ronchi ruling periods is very small (see Table 3.1.1) compared to the usual sizes of the exit pupil to the surface. The superimposed area is thus quite close to the full area of pupil being tested. A number of lateral shearing interferometers for metrological applications, based on Ronchi rulings, have been proposed [Schreiber 1997][Hibino 1997].

Table 3.1.1: Amount of shear introduced between displaced images of the exit pupil of the surface being tested, for typical periods of the ruling ($\lambda=635\text{nm}$, $f'=50\text{mm}$, $n=1$).

Ruling period (mm)	0.508	0.254	0.127	0.085
Shear $\lambda f'/T$ (mm)	0.063	0.125	0.250	0.375

3.1.3.- Incident spherical wave

Let's continue our description of the Ronchi test assuming some kind of incident wavefront. We shall assume that a perfect diverging spherical wavefront of radius D_r is reaching the Ronchi test. That is, let

$$U_R(x_R, y_R) = \frac{A}{\Delta r} e^{-i \frac{k}{2\Delta r} (x_R^2 + y_R^2)} \quad (3.1.8)$$

By using the scaling property of the Fourier transform, combining Eq.(3.1.7) and Eq.(3.1.8)

$$U_f(x_f, y_f) = -\frac{A}{f'} \cdot e^{i \frac{k}{2f'} (1 - \frac{d}{f'}) (x_f^2 + y_f^2)} \sum_{n=-\infty}^{\infty} B_n \cdot e^{i \frac{\pi \Delta r}{\lambda f'^2} \left[\left(x_f - \frac{n\lambda f'}{T} \right)^2 + y_f^2 \right]} \quad (3.1.9)$$

$$\text{Defining } R_o = \frac{f'^2}{\Delta r}$$

$$U_f(x_f, y_f) = -\frac{A}{f'} \cdot e^{i \frac{k}{2f'} (1 - \frac{d}{f'}) (x_f^2 + y_f^2)} \sum_{n=-\infty}^{\infty} B_n \cdot e^{i \frac{\pi}{\lambda R_o} \left[\left(x_f - \frac{n\lambda f'}{T} \right)^2 + y_f^2 \right]} \quad (3.1.10)$$

So, except for the phase and amplitude factors common to all the diffracted orders that are being superimposed, the result of the incidence of a spherical wavefront on a Ronchi ruling is the superposition of an infinity of spherical waves with radius R_o , amplitude B_n and centered at $x_f = \frac{n\lambda f'}{T}$, $y_f=0$. This result will be recalled in Section 3.2.3 in order to justify the geometrical interpretation of the Ronchi test in our experimental setup. It also shows that the detected fringes on the CCD array will not be sharp, as interference between many of the diffracted orders will blur them.

A further interpretation of this result [Malacara 1990] may be achieved by rewriting Eq. 3.1.9 developing the exponential term:

$$U_f(x_f, y_f) = -\frac{A}{f'} \cdot e^{i \frac{k}{2f'} (1 - \frac{d}{f'} + \frac{\Delta r}{f'}) (x_f^2 + y_f^2)} \sum_{n=-\infty}^{\infty} B_n \cdot e^{-i \frac{2\pi n \Delta r}{T f'} x_f} e^{i \frac{\pi \Delta r}{\lambda f'^2} \left(\frac{n\lambda f'}{T} \right)^2} \quad (3.1.11)$$

Eq. 3.1.11 shows how each of the diffracted orders may be considered as a plane wave propagating in a direction α with the Z axis, with $\sin \alpha = \frac{2\pi n \Delta r}{T f'}$, and a phase term dependent on n^2 that equals the optical path difference (OPD) between two

spherical wavefronts of radius $\frac{f'^2}{\Delta r}$ with its centers sheared a distance $\frac{n\lambda f'}{T}$ along X_1 axis.

3.1.4.- Talbot planes

As a consequence of Eq. (3.1.11) we may see that there are a set of positions along the Z axis where the OPD term equals $2m\pi$, namely

$$2m\pi = \frac{\pi \Delta r}{\lambda f'^2} \left(\frac{n\lambda f'}{T} \right)^2 = \pi \cdot \Delta r \frac{n^2 \lambda}{T^2} \quad (3.1.12)$$

So the condition for the OPD term of Eq. 3.1.11 to equal unity is

$$\Delta r = \frac{2m T^2}{n^2 \lambda} \quad (3.1.13)$$

At these positions along the Z axis, the optical path difference between the non-diffracted wavefront and the n^{th} term of the superposition differ an integer multiple of 2π , so the superposition of these orders will be equal to that of two tilted plane waves. The interference between these two components of the diffracted wavefront would give rise to well-defined, straight sinusoidal fringes.

This is the Talbot effect applied to Ronchi deflectometry. It occurs when one of the diffracted orders has a shift along X_1 axis equivalent to the ruling spacing projected on the observation plane [Latimer 1992]. This effect has been theoretically simulated for the special case of the Ronchi test [Berry 1996], and widely used in measurement applications [Nakano 1985][Oreb 1994].

The Talbot effect, however, would be especially noticeable when the orders, shifted $2m\pi$ radians, fulfill two conditions: they should carry as much energy as possible and they should interfere with contrast as high as possible. The contrast of the fringes will decrease as the amplitude difference between the interfering orders increases. Table 3.1.2 shows the contrast and energy values for the interference between some of the sheared diffracted orders, obtained from their amplitudes B_n and B_n' . Energy I_0 is obtained as the square root of the sum of the squared amplitudes.

It may now be seen that the term with highest contrast combined with highest energy will be the interference between the zero order and the first order. By placing $n=1$ in 3.1.13 we obtain the set of points on Z axis

$$\Delta r = 2m \frac{T^2}{\lambda} \quad (3.1.14)$$

which is the set of distances from the center of curvature in which the sharpness of the Ronchi fringes obtained will be greatest. Another set of fringes with maximum sharpness may be obtained for values of the OPD term equal to $m\pi$, that is

$$\Delta r = (2m + 1) \frac{T^2}{\lambda} \quad (3.1.15)$$

In these positions, fringes will display a contrast reversal in respect of the fringes in positions described by Eq. (3.1.14). It may also be seen that at the set of positions

$$\Delta r = \frac{(2m + 1) T^2}{2 \lambda} \quad (3.1.16)$$

the contrast of the fringes will be minimum, as the phase difference between the first and zero orders is $(2m+1)\pi/2$.

Table 3.1.2: Relative energy (I_0) and contrast (C) of hypothetical interference between some pairs of diffracted orders. Values calculated from B_n coefficients, so even diffracted orders have no amplitude (See Eq. 3.1.5).

n=0	n'	1	3	5	7	9
	C	90.6	40.6	25.1	18.0	14.1
	I_0	0.351	0.261	0.254	0.252	0.251
n=1	n'	3	5	7	9	11
	C	60.0	38.5	28.0	21.9	18.0
	I_0	0.112	0.105	0.102	0.102	0.102
n=3	n'	5	7	9	11	13
	C	88.2	72.4	60.0	50.8	43.8
	I_0	0.015	0.013	0.013	0.012	0.012

3.2 Geometrical theory of the Ronchi test

The Ronchi test may be interpreted geometrically as well as by the diffractive theory developed until now. The geometrical approach is simpler, because it describes the fringe patterns obtained merely as projections of the Ronchi test bands, but it does not take into account the diffractive effects described in Section 3.1.

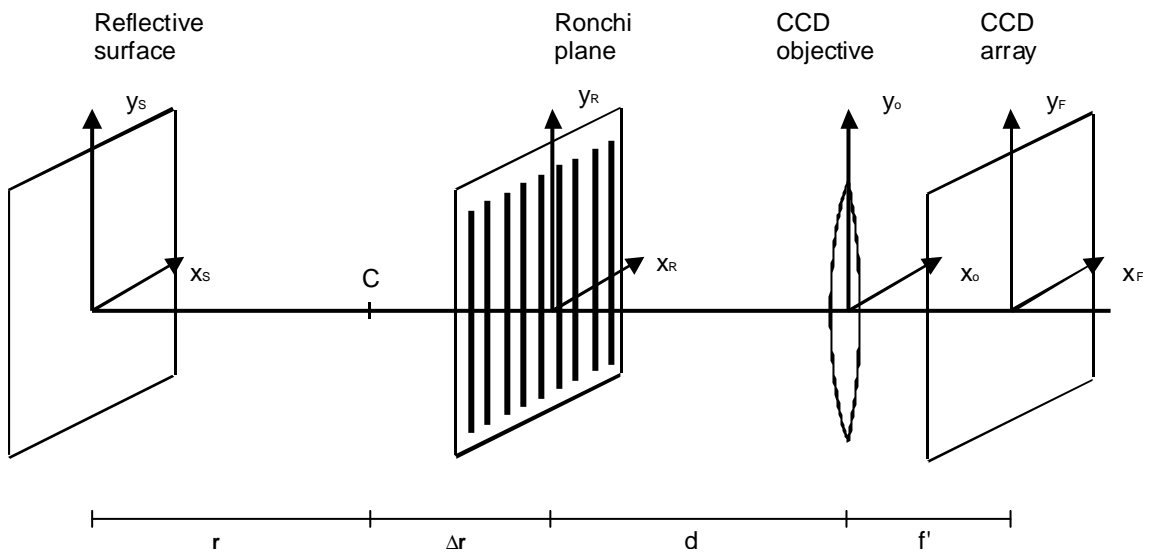
Furthermore, the diffractive theory developed along the previous Section must be implemented starting at the focal point of the wavefront being considered, as this point is a singular one. Direct information from the surface may not then be obtained. The geometrical theory, as a ray propagation approach, will not be affected by this situation, allowing profilometry of reflective surfaces.

3.2.1.- Geometrical theory of the Ronchi test

When no diffractive effects are taken into account, light may be assumed to travel along rays, the basis of the geometrical theory. We shall consider the setup and reference systems described in Fig.3.2.1, which are intentionally kept equivalent to the ones in Fig.3.1.1. Let the wavefront being measured be described for a function $W(x_S, y_S)$, and let the reference system $X_S Y_S$ define the $z=0$ plane. The normal vectors to the wavefront leaving the surface will be

$$\vec{n}_r(x_S, y_S) = \vec{\nabla} \cdot W(x_S, y_S) = \left[\frac{\partial W(x_S, y_S)}{\partial x_S}, \frac{\partial W(x_S, y_S)}{\partial y_S}, \sqrt{1 - \left(\frac{\partial W(x_S, y_S)}{\partial x_S} \right)^2 - \left(\frac{\partial W(x_S, y_S)}{\partial y_S} \right)^2} \right] \quad (3.2.1)$$

Fig. 3.2.1: Reference systems used to develop the geometrical theory of the Ronchi test. Names and positions have been kept identical to those used in Section 3.1.



For small apertures, the z component of the normal vector may be considered unity. This is the direction of the rays leaving the tangent plane to the surface. At each point (x_S, y_S) we may thus find the ray equation

$$\frac{x - x_S}{\frac{\partial W(x_S, y_S)}{\partial x_S}} = \frac{y - y_S}{\frac{\partial W(x_S, y_S)}{\partial y_S}} = z \quad (3.2.2)$$

provided the component of the normal vector is equal to unity and the $X_S Y_S$ plane is placed at $z=0$. So on any given plane placed a distance z away from the tangent plane to the surface, the rays leaving the surface will intersect at coordinates given by

$$\begin{aligned} x &= x_S + z \frac{\partial W(x_S, y_S)}{\partial x_S} \\ y &= y_S + z \frac{\partial W(x_S, y_S)}{\partial y_S} \end{aligned} \quad (3.2.3)$$

So, in particular, on the Ronchi plane $X_R Y_R$

$$\begin{aligned} x_R &= x_S + (r + \Delta r) \frac{\partial W(x_S, y_S)}{\partial x_S} \\ y_R &= y_S + (r + \Delta r) \frac{\partial W(x_S, y_S)}{\partial y_S} \end{aligned} \quad (3.2.4)$$

where the small angle approximation has been assumed. Under this approximation relationships between each of the reference systems may be found [Casas 1985]

$$\begin{aligned} \frac{x_S}{r} &= \frac{x_R}{\Delta r} = \frac{x_o}{d + \Delta r} = \frac{x_f}{f'} \\ \frac{y_S}{r} &= \frac{y_R}{\Delta r} = \frac{y_o}{d + \Delta r} = \frac{y_f}{f'} \end{aligned} \quad (3.2.5)$$

where the small angle approximation has been taken into account.

So the intersection of each ray on the tangent plane to the surface with the CCD array will be given by

$$\begin{aligned} x_f &= \frac{f'}{\Delta r} x_R = \frac{f'}{\Delta r} x_S + f' \frac{(r + \Delta r)}{\Delta r} \frac{\partial W(x_S, y_S)}{\partial x_S} \\ y_f &= \frac{f'}{\Delta r} y_R = \frac{f'}{\Delta r} y_S + f' \frac{(r + \Delta r)}{\Delta r} \frac{\partial W(x_S, y_S)}{\partial y_S} \end{aligned} \quad (3.2.6)$$

The shape of the final shadow pattern may then be described and calculated for any incident wavefront. Each of the lines in the Ronchi test can be expressed by

$$\begin{aligned} x_R &= mT \\ y_R &= y_R \end{aligned} \quad (3.2.7)$$

and through Eq.3.2.5, Eq. 3.2.6 and Eq. 3.2.7

$$\begin{aligned} x_f &= m \frac{f'r}{\Delta r^2} T + f' \frac{(r + \Delta r)}{\Delta r} \frac{\partial W(x_S, y_S)}{\partial x_S} \\ y_f &= \frac{f'r}{\Delta r^2} y_S + f' \frac{(r + \Delta r)}{\Delta r} \frac{\partial W(x_S, y_S)}{\partial y_S} \end{aligned} \quad (3.2.8)$$

A full study of the shapes in the shadow pattern caused by each of the Seidel aberrations, or its combinations, may be performed using Eq.3.2.8 [Adachi 1960a][Cornejo 1992], and the quantitative measurement of the aberrations present in a given wavefront is also possible [Adachi 1960b].

Another common use of Eq.3.2.6 and eq.3.2.8 is the development of the so-called "null tests". A null test is a Ronchi test where the straight lines have been replaced with curves that, for the particular wavefront being tested, should give straight shadows at the final plane. Possible deformations in the wavefront are then easier to detect [Cordero 1990][Malacara 1974].

3.2.2.- Equivalence of geometrical and diffractive theories

So far the geometrical and diffractive theories of the Ronchi test have been presented. We will now show how both theories are equivalent under certain experimental conditions.

We shall recover Eq. 3.1.11, gathering the terms outside the sum in a complex constant $C(x_f, y_f)$:

$$U_f(x_f, y_f) = C(x_f, y_f) \sum_{n=-\infty}^{\infty} B_n \cdot e^{-i \frac{2\pi n \Delta r}{T} x_f} e^{i \frac{\pi \Delta r}{\lambda f'^2} \left(\frac{n \lambda f'}{T} \right)^2} \quad (3.2.9)$$

Rewriting the exponential term, this equals

$$U_f(x_f, y_f) = C(x_f, y_f) \sum_{n=-\infty}^{\infty} B_n e^{-i \frac{2\pi n \Delta r}{T} \frac{\Delta r}{f'} \left(x_f - \frac{n \lambda f'}{2T} \right)} \quad (3.2.10)$$

Now we recall Eq. 3.1.5, the original Fourier series representing the unit amplitude square wave profile, to see that Eq. 3.2.10 is merely the expression of a sum of scaled square wave profiles, with a shear along the x_f plane. That is, on the focal plane of the objective we find a superposition of sheared projections of the original transmittance profile.

From the point of view of geometrical optics, a projected and scaled pattern of the original transmittance profile is what we would expect to obtain in the final intensity pattern. So the geometrical theory will be valid when the shear values are small enough, when compared with the size of the intensity profile.

A condition may therefore be imposed on the amount of shear of the first diffracted order to establish a theoretical threshold for the validity of the geometrical approach. Our supposition has been assuming that

$$\frac{\lambda f'}{2T} < \frac{T}{8} \quad (3.2.11)$$

Assuming typical values in our experimental setup ($\lambda=635\text{nm}$, $f'=50\text{mm}$):

$$T > 0.356\text{mm} \quad (3.2.12)$$

For shorter periods diffractive effects need to be taken into account as they may affect the measurements. In frequency terms, this means that geometrical and diffractive theories may be considered equivalent when using ruling frequencies under 3 lines per mm (70 lines per inch). A similar approach is presented in [Cornejo 1970].

This equivalence may be further confirmed by comparing the results predicted for both theoretical models for the shadows of the ruling registered on the CCD array. The geometrical theory establishes a plane to plane relationship described in Eq. 3.2.5, which states

$$x_f = \frac{f'}{\Delta r} x_r \quad (3.2.13)$$

So on the focal plane of the objective, one period of the Ronchi ruling sizes

$$\Delta x_f = \frac{f'}{\Delta r} T \quad (3.2.14)$$

Using the diffractive theory with low frequency rulings allows us to write, from Eq. 3.2.10:

$$U_f(x_f, y_f) \approx C(x_f, y_f) \sum_{n=-\infty}^{\infty} B_n e^{-i \frac{2\pi n}{T} \frac{\Delta r}{f'} x_f} = C(x_f, y_f) \sum_{n=-\infty}^{\infty} B_n e^{-i \frac{2\pi n}{T_{\text{eq}}} x_f} \quad (3.2.15)$$

The last expression is the Fourier series representing a square wave with period T_{eq} . It follows that the period of the complex amplitude distribution at $X_f Y_f$ is

$$T_{\text{eq}} = \frac{f'}{\Delta r} T \quad (3.2.16)$$

By looking at Eq. 3.2.14 it may be seen that, under the aforementioned frequency conditions, geometrical and diffractive theories give equivalent results.

3.3 Surface profile measurements

Both the geometrical and the diffractive theory of the Ronchi test have now been discussed. The first approach is simpler, because it describes the shadow patterns obtained simply as projections of the Ronchi test bands, but fails to take into account the diffractive effects, which may be significant in some cases. The physical diffractive theory is valid in a wider set of conditions, but it is rather awkward to work with.

In the following paragraphs experimental conditions allowing the equivalence of both theories are assumed (see Section 3.2.2), as these frequency values will be the usual in our experimental setup. Geometrical theory will consequently be used for the sake of simplicity. With this approach, the registered pattern on the CCD array will be called a "shadow pattern", as the diffractive behavior giving a "fringe pattern" has been shown to be negligible under these experimental conditions.

3.3.1.- Ray aberration, wave aberration and surface measurements

Before applying our analysis to the measurement of a surface profile, a few remarks on wavefront aberration measurement and its relationship to surface measurements will be made. We will show how measurements of transverse ray aberration may be related to surface deformations.

The Ronchi test has been shown to be a direct way to measure the transverse ray aberration of a wavefront [Cornejo 1992], which is the departure from an ideal point of the image of the wavefront on a given plane, in our case the Ronchi plane. Ray aberration measurements may be translated into wave aberration values through the exact relations [Rayces 1964]

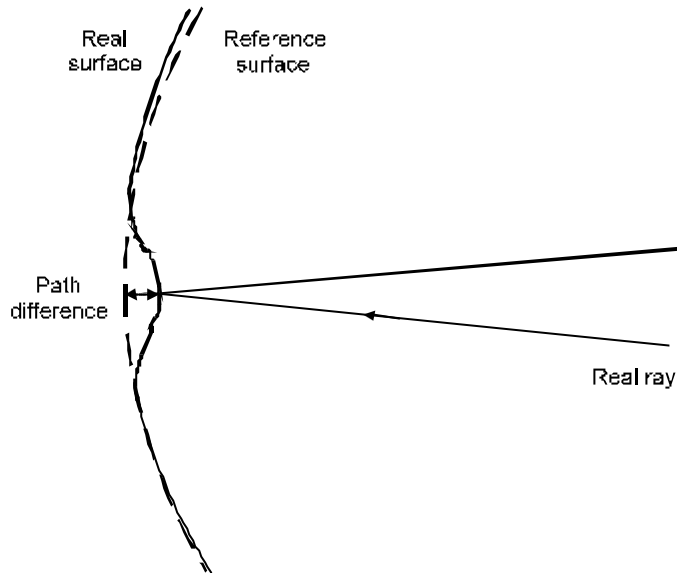
$$\begin{aligned} \frac{\partial W(x_R, y_R)}{\partial x_R} &= \frac{TA_x}{R - W(x_R, y_R)} \\ \frac{\partial W(x_R, y_R)}{\partial y_R} &= \frac{TA_y}{R - W(x_R, y_R)} \end{aligned} \quad (3.3.1)$$

where $W(x_R, y_R)$ is the wave aberration function, i.e, the departure of the wavefront from a reference sphere of known radius R at the Ronchi ruling plane. $X_R Y_R$ is the reference system on the Ronchi plane, as in previous Sections.

This wave aberration function is none other than the optical path difference (OPD) function from the reference surface on the plane where the transverse ray aberration was measured. If this wavefront is coming from a reflective surface, the wavefront deviation from the ideal shape will be twice the deviation existing on the

surface, as the path covered by the wavefront is twice the path covered along the surface (Fig.3.3.1).

Fig.3.3.1: The optical path difference on the wavefront (OPD) is twice the height difference on the surface.



3.3.2.- Surface reconstruction through the Ronchi test

The geometrical theory described will be used in order to measure the profile of a concave reflective surface. Given the shape of the wavefront impinging on the surface to be measured, local deformations on the reflected wavefront allow local information on the shape of the surface to be obtained. This local shape is found through indirect measurements of the local normal vector to the surface, as each of the rays of the incident wavefront will be reflected in an angle related to the normal at the incidence point.

The information required to obtain a full three-dimensional topographic surface profile will be the shadow pattern registered on a CCD array, and the relative positions of the light source and the surface relative to the Ronchi ruling. The setup assumed is presented in Fig.3.3.2.

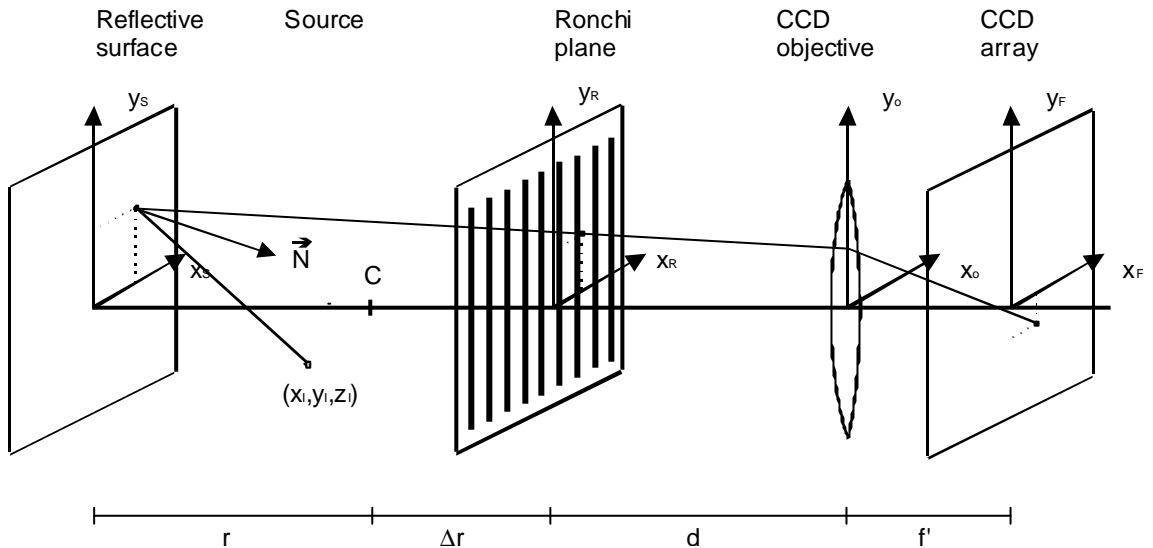
We shall start from the shadow pattern present in the CCD array. As this has been placed on the focal plane of the objective lens pointing at infinity, each position in the CCD array may be related to a slope along both axes. This slope is the directive cosine of the ray incident on the objective (X_0Y_0 plane). The direction of the ray incident at (x_i, y_i) must be

$$\bar{s}_R = \left(\frac{x_f}{f'}, \frac{y_f}{f'}, \sqrt{1 - \left(\frac{x_f}{f'}\right)^2 - \left(\frac{y_f}{f'}\right)^2} \right) \approx \left(\frac{x_f}{f'}, \frac{y_f}{f'}, 1 \right) \quad (3.3.2)$$

if the small angle approximation is assumed to be valid.

If we had the (x_R, y_R) coordinates of the intersection of this ray with the plane $z=r+\Delta r$, the full equation for the ray would be known. Section 4 will describe in detail how these coordinates are obtained. For the time being we will simply point out that the position of the shadows on the pattern recorded at $X_f Y_f$ allows us to find the position where a ray with a given slope intersects the Ronchi plane. In the Fig.3.3.2 setup the x_R coordinate would be obtained. By placing the ruling lines along X_R , we would obtain y_R .

Fig.3.3.2: Measurement of the local normal vectors of a reflective surface using Ronchi deflectometry.



Once a point and the direction of the ray have been measured, the ray equation may be written as

$$\frac{x - x_R}{x_f/f'} = \frac{y - y_R}{y_f/f'} = z - (r + \Delta r) \quad (3.3.3)$$

Remaining in the small angle approximation, the whole surface is assumed to be a plane placed at $z=0$, that is, the plane tangent to the surface at its vertex. By applying Eq.3.3.3 to the special case of $(x_s, y_s, 0)$, the intersection of the ray with the surface may be shown to be

$$\begin{aligned}x_s &= x_R - \frac{r + \Delta r}{f'} x_f \\y_s &= y_R - \frac{r + \Delta r}{f'} y_f\end{aligned}\tag{3.3.4}$$

Now we may use the known coordinates of the source to calculate the directive cosines for the ray incident on the surface at that point. Given that the source is placed at (x_i, y_i, z_i) , the incident ray will have a direction

$$s_i = \left(\frac{x_i - x_s}{z_i}, \frac{y_i - y_s}{z_i}, 1 \right)\tag{3.3.5}$$

As the directions of the incident and reflected ray are known, the components of the normal vector may be calculated using Eq.3.3.2 and Eq.3.3.5 as

$$\begin{aligned}N_x &= \frac{1}{2} [s_{Rx} + s_{Ix}] = \frac{x_f}{2f'} \left[1 + \frac{r + \Delta r}{z_i} \right] + \frac{1}{2z_i} [x_i - x_R] \\N_y &= \frac{1}{2} [s_{Ry} + s_{Iy}] = \frac{y_f}{2f'} \left[1 + \frac{r + \Delta r}{z_i} \right] + \frac{1}{2z_i} [y_i - y_R]\end{aligned}\tag{3.3.6}$$

So the normal to the surface at a set of points may be obtained using the known source position (x_i, y_i, z_i) , and the measured values for (x_R, y_R) and (x_f, y_f) .

The values of the local normal will so be obtained at a set of points over the sampled surface. Integration of the local normals will allow the topographic reconstruction of the measured area of the surface under test, from which it will be possible to measure the parameters which describe the surface (typically, its radius of curvature) through curve-fitting. Detailed account on the integration and the remaining data processing steps will be given along the following Section of this work.